

# Journal of Materials Chemistry C

Accepted Manuscript



This is an *Accepted Manuscript*, which has been through the Royal Society of Chemistry peer review process and has been accepted for publication.

*Accepted Manuscripts* are published online shortly after acceptance, before technical editing, formatting and proof reading. Using this free service, authors can make their results available to the community, in citable form, before we publish the edited article. We will replace this *Accepted Manuscript* with the edited and formatted *Advance Article* as soon as it is available.

You can find more information about *Accepted Manuscripts* in the [Information for Authors](#).

Please note that technical editing may introduce minor changes to the text and/or graphics, which may alter content. The journal's standard [Terms & Conditions](#) and the [Ethical guidelines](#) still apply. In no event shall the Royal Society of Chemistry be held responsible for any errors or omissions in this *Accepted Manuscript* or any consequences arising from the use of any information it contains.

# Piezoresistance in $\text{Si}_3\text{N}_4$ Nanobelts: Toward Highly Sensitive and Reliable Pressure Sensors

*Jinghui Bi<sup>1,2,3</sup>, Guodong Wei<sup>2</sup>, Minghui Shang<sup>2</sup>, Fengmei Gao<sup>2</sup>, Bin Tang<sup>1,\*</sup>, and Weiyu Yang<sup>2,\*</sup>*

<sup>1</sup> Research Institute of Surface Engineering, Taiyuan University of Technology, Taiyuan City 030024, P.R. China.

<sup>2</sup> Institute of Materials, Ningbo University of Technology, Ningbo City 315016, P.R. China.

<sup>3</sup> College of Applied Science, Taiyuan University of Science and Technology, Taiyuan City 030024, P.R. China.

---

\* Corresponding author: E-mails: [tangbin@tyut.edu.cn](mailto:tangbin@tyut.edu.cn) (B. Tang) and [weiyuyang@tsinghua.org.cn](mailto:weiyuyang@tsinghua.org.cn) (W. Yang)

## Abstract

For the purposes of precision instrumentation and accurate measurement, there is a growing need for pressure sensors to be well serviced in harsh environments. In the present work, we report, for the first time, the piezoresistance in single-crystalline Si<sub>3</sub>N<sub>4</sub> nanobelts via a conductive atomic force microscopy (C-AFM). The transverse electromechanical properties of the Si<sub>3</sub>N<sub>4</sub> nanobelt were investigated under various loading forces applied by the tip of C-AFM. The transverse piezoresistance coefficient  $\pi_{[1\bar{2}0]}$  of the nanobelt is calculated to be in the range of 2.2 to  $8.8 \times 10^{-11}$  Pa<sup>-1</sup> under the applied loading forces from 25.6 to 135.3 nN. The relationship between the piezoresistance coefficients and applied forces is almost linear. The significant and linear decreases of the nanobelt resistances with the increase of the loading forces have been observed, which exhibit a variation of  $\sim 3$  M $\Omega$  with a changed force of 1 nN, implying that the pressure sensors possess a high sensitivity. Stable and repeatable  $I$ - $V$  curves through multiple voltage sweepings can be accomplished, suggesting that the Si<sub>3</sub>N<sub>4</sub> nanobelts pressure sensors are highly reliable.

## 1. Introduction

Semiconductor sensors are distinguished by large piezoresistive coefficients, and therefore have been applied widely in the measurement of pressure, strain, flow, acceleration, and force. Recently, pressure sensors based on one-dimension (1D) nanostructures have attracted more and more attention, due to the giant piezoresistive effect derived from the reduced dimensions of nanomaterials compared to those of their conventional bulk counterparts.<sup>1,2</sup> Up to date, carbon nanotubes,<sup>3-5</sup> Si nanowires,<sup>1,6</sup> ZnO nanostructures,<sup>7-12</sup> SiC nanowires<sup>13-15</sup> and *et al.* were extensively used as the functional units to construct various pressure sensors, showing that 1D semiconductors can be a superior candidate for detecting nN-scale force in the nanoelectromechanical system (NEMS) devices.

For the purposes of precision instrumentation and accurate measurement, there is a growing need for sensing devices to be well serviced in harsh environments, *e.g.*, in satellites, space, volcano and so forth. The emerging challenges are that the fabricated devices are required to have following abilities: i) well work ability under high temperatures (>200 °C); ii) excellent resistance to acid and alkali conditions as well as strong radiation environments. Similar to III-N semiconductors, Si<sub>3</sub>N<sub>4</sub> possesses wide-band-gap semiconducting behavior and could be an excellent host material due to its excellent mechanical performances,<sup>16-18</sup> wide-band-gap structure, thermomechanical properties and chemical inertness,<sup>19-21</sup> which could enable them a very promising candidate to be serviced under high-temperature harsh conditions. Currently, many efforts were put for the synthesis of 1D Si<sub>3</sub>N<sub>4</sub> nanostructures in various morphologies,<sup>22-27</sup> which showed their unique applications in optics,<sup>28,29</sup> field-effect transistors,<sup>30</sup> and so on. However, to the best of our knowledge, there is no any works focused on the electromechanical properties of Si<sub>3</sub>N<sub>4</sub> nanostructures.

Here, we reported, for the first time, the piezoresistance behaviors in high-qualified single-crystalline  $\text{Si}_3\text{N}_4$  nanobelts under various applied loading forces via a C-AFM. The transverse electromechanical properties of the nanobelts were investigated, and the mechanism for the piezoresistive effect was proposed. The experimental results suggested that current work might open a new door for the exploration of novel pressure sensors with high sensitivity and reliability by using  $\text{Si}_3\text{N}_4$  nanobelts as the functional units.

## 2. Experimental Procedure

Currently used  $\alpha\text{-Si}_3\text{N}_4$  nanobelts were synthesized via pyrolysis of a polyaluminasilazane precursor using Al powders as the catalysts, which were reported detailedly in our previous work.<sup>31</sup> For characterization of their electromechanical properties, a drop of alcohol solution containing the as-synthesized  $\text{Si}_3\text{N}_4$  nanobelts was dripped onto a metallic highly oriented pyrolytic graphite (HOPG) substrate, followed by being dried in the vacuum oven at 60 °C. The nanobelts were characterized using field emission scanning electron microscopy (FESEM, S-4800, Hitachi, Japan). The electromechanical measurements were performed using a conductive atomic force microscopy (C-AFM, Nanoscope V, Veeco, USA) with Pt/Ir-coated tips (force constant: 0.2 N/m) at room temperature.

## 3. Results and Discussion

Fig. 1(a-b) show the typical SEM images of the as-synthesized  $\alpha\text{-Si}_3\text{N}_4$  nanobelts under different

magnification, suggesting the large-scale growth of the nanobelts with typical lengths in the range of tens to hundreds of micrometers. The bending nanobelts (Fig. 1(a)) reveal that these belts are highly flexible. According to the selected area electron diffraction (SAED) analysis (Fig. S1, Electronic Supplementary Information),<sup>31</sup> the belts grow along [101] direction with a top surface of  $(1\bar{2}0)$ , which are schematically shown in Fig. 1(c-d) in various view angles.

The transverse piezoresistance characterizations of a single  $\text{Si}_3\text{N}_4$  nanobelt were examined by the C-AFM with Pt/Ir-coated tips (force constant: 0.2 N/m) at room temperature, which is schematically shown in Fig. 2(a). The AFM tip was fixed on the top of the single nanobelt lying on the HOPG substrate, leading to the formation of Pt/Ir-SiN-graphite structure, which can be regarded as a typical metal-semiconductor-metal (M-S-M) architecture. As compared to the conventional single 1D nanostructure device by terminating the electrodes at nanowire ends, the present architecture have following merits: i) Low cost and time saving. Currently, the configurations of single nanostructure devices are usually performed by electron-beam lithography (EBL), which always result in a high cost and low efficiency; ii) Good electric contact. The contact between the electrodes and 1D nanostructure ends may be unstable due to the limited contact area. Because the nanobelt lies on the graphite substrate, which could make its entire down surface effectively contact the graphite electrode, and thus offer our architecture having the best contact in theory; iii) Benefit to the study of the current transport at nanoscale. In conventional devices, the current transport is often through the entire length of nanowire, which is often the order of micrometer or even longer. In our system, the path is dependent on the thickness of nanobelt, which can be conveniently adjusted by choosing the nanobelts with different thicknesses. Also, the short path can effectively get rid of the influence of defects and Joule effect. Fig.

2(b) depicts a typical AFM image of a single Si<sub>3</sub>N<sub>4</sub> nanobelt lying on the graphite substrate, which is 50 nm in thickness (Fig. 2(c)). The work functions of Si<sub>3</sub>N<sub>4</sub> semiconductor, graphite and Pt/Ir tip are ~4.75 eV, 4.40 eV<sup>32</sup> and 5.10 eV,<sup>33</sup> respectively. Thus, the SiN-graphite contact is Ohmic at the bottom, and the Pt/Ir-SiN contact should be Schottky with a barrier height of ~1.0 eV at the top surface.

Fig. 2(d) displays the *I-V* curves of the Pt/Ir-tip/nanobelt/graphite configuration at various loaded forces ranged from 25.6 nN to 135.3 nN. The nonlinearity and asymmetric behaviors of the *I-V* curves together with the high turn-on voltages disclose that the AFM-tip/SiN junction is not an Ohmic contact but a Schottky one. It seems that, at a low loading force of 25.6 nN, a clear rectifying behavior within the large voltage range can be observed, which is consistent with the Schottky contact for the present metal-semiconductor-metal system. At the same negative bias, the current density is found to increase significantly with the raise of the applied loading force. The positive current density also presents the same tendency, and increases with the raise of the loading forces under the same bias.

In order to explain the phenomena observed in Fig. 2(d), the *I-V* curves under the negative bias were analyzed by using the theory of piezoresistance effect. The change of the resistance induced by the external strain fixed on the surface of (1  $\bar{2}$  0) of the Si<sub>3</sub>N<sub>4</sub> nanobelt can be given by:

$$\pi_{[\bar{1}20]} = \frac{\Delta R S}{R_0 F} \dots\dots\dots (1)$$

where  $\Delta R$  is the resistance change between the ones with and without an external force,  $\pi_{[\bar{1}20]}$  is the piezoresistance coefficient,  $R_0$  is the resistance under zero force,  $F$  is the applied force,  $S$  is the contact area between the spherical AFM tip and nanobelt, which can be approximately calculated by the deformation  $\Delta h$  of Si<sub>3</sub>N<sub>4</sub> nanobelt along the transverse direction. According to the Hertz model used for

a half-space in contact with a spherical tip,<sup>34</sup>  $\Delta h$  can be expressed as:

$$\Delta h = \left( \frac{9F^2}{16Y_{eff}^2 r_{tip}} \right)^{1/3} Q(r_{tip}) \dots \dots \dots (2)$$

where  $Y_{eff}$  is the effective Young's modulus, and  $Q$  is the geometric factor. Combining with Eq. (1-2),

the piezoresistance coefficient of  $\pi_{[120]}$  can be given by:

$$\pi_{[120]} = \frac{2\pi_{tip}\Delta R}{FR_0} \left( \frac{9F^2}{16Y_{eff}^2 r_{tip}} \right)^{1/3} Q(r_{tip}) \dots \dots \dots (3)$$

With the  $Y_{eff}$  of  $\text{Si}_3\text{N}_4$  nanobelt being of  $\sim 570$  GPa.<sup>17</sup> Eq. (3) can be simplified as:

$$\pi_{[120]} = k \frac{\Delta R}{F^{1/3} R_0} \dots \dots \dots (4)$$

where  $k$  is a constant of *ca.*  $5.56 \times 10^{-13}$ . Consequently, the piezoresistance coefficient  $\pi_{[120]}$  of the nanobelt can be calculated out, which falls in the range of 2.17 to  $8.8 \times 10^{-11}$  Pa<sup>-1</sup> under the applied loading forces from 25.6 to 135.3 nN. These transverse piezoresistance coefficients are comparable to the longitude one of ultra-strained SiC nanowire with a diameter of  $\sim 150$  nm,<sup>14</sup> which is also a promising high temperature sensor candidate. Meanwhile, it should be pointed out that the piezoresistance coefficient in present study is just for the nanobelt with 50 nm thickness. Since the transverse conductance and band gap variations of the nanobelts are a function of the belt thicknesses, the piezoresistance coefficient of nanobelt with smaller thickness (*e.g.*  $< 10$  nm) may be greatly enhanced.

As a promising pressure sensor, besides the high piezoresistance coefficient, it should have the almost the linear electromechanical properties as well as high sensitivity and robust reliability. Fig. 3(a) shows the relationship of the resistances *vs.* loaded forces. For eliminating the contact resistance, the resistances of  $\text{Si}_3\text{N}_4$  nanobelt can be calculated from the linear sections of the  $I$ - $V$  curves in Fig. 2(d) by



using the equation of  $R = \Delta V / \Delta I$ , where  $\Delta V$  is the voltage variations between two measured points in the linear sections under the negative bias, and  $\Delta I$  is the corresponding current change.<sup>35</sup> It is noted that the decrease in the resistance of the nanobelt is almost linear to the applied force. As shown in Fig. 3(a), the resistances can be greatly reduced from 470 to 50 M $\Omega$  with the increase of the loading forces from 0 to 135 nN. It strongly suggests that current pressure sensor exhibits a high sensitivity with a resolution of 1 nN force or even 0.1 nN. In other words, applied 1 nN force on the nanobelt can result in a variation of  $\sim 3$  M $\Omega$  in the resistance. Such a large variation can be easily detected by electrical method. In addition, the fact of large variation of resistances also means that the strain can significantly increase the electron concentration and the conductivity of Si<sub>3</sub>N<sub>4</sub> nanobelt along the transverse direction. Fig. 3(b) shows the curve of the piezoresistance coefficients vs. applied forces, implying that the relationship between piezoresistance coefficient and force is almost linear. Fig. 3(c) depicts the  $I$ - $V$  curves with the bias voltage sweeping direction followed the arrows under a fixed applied external force of 43.9 nN, suggesting that stable and repeatable  $I$ - $V$  curves through multiple voltage sweepings can be achieved. No hysteresis behavior indicates that the sensor can be a damage-free sensor and can be fully and quickly recovered once the compressed stress released. Similar measurements with different contact points along the nanobelt were carried out, and the measured  $I$ - $V$  curves are almost identical, implying that our Si<sub>3</sub>N<sub>4</sub> nanobelts could be an excellent candidate for the exploration of reliable pressure sensors.

It is generally accepted that the piezoresistance effect can be explained by the strain-induced band structure change and the mobility shift in bulk semiconductors. As for the counterparts in nanoscale, there are three possible mechanisms accounting for the origination of piezoresistance effect:

1) surface quantization effect occurred in the first few surface monolayers;<sup>36</sup> 2) stress-induced change of

surface state;<sup>37</sup> 3) band structure change caused by the strain.<sup>14,38</sup> Given the fact that the thickness of the as-synthesized nanobelt are beyond the Bohr radius (<10 nm), the contribution from the quantum confinement can be ignored. Here, we infer that the piezoresistance behaviors of Si<sub>3</sub>N<sub>4</sub> nanobelts could be mainly caused by the change of surface state and band structure.<sup>36</sup> According to the reported works,<sup>36</sup> the surface and interior regions have opposite reaction to the deformation at the tip contact point. Such opposite reaction induces the change of surface state, resulting in the variation of the resistance. On the other hand, under a loading force, the band gap of Si<sub>3</sub>N<sub>4</sub> nanobelt could be changed,<sup>39</sup> making the change of the resistance of nanobelt and Schottky barrier height between the nanobelt and electrode. According to the classic thermionic emission-diffusion theory,<sup>40</sup> the slight decrease of the Schottky barrier height can induce a large increase of the negative current density as observed in Fig. 2(d), due to the exponential function relation between them. The increase of the positive current density could also be explained by the same theory. In addition, considering that a large number of vacancies or absorbed oxygen can be often around the nanobelt surface, the contribution from tunneling through the Schottky barrier could also exist, and thus the tunneling current cannot also be negligible.

#### 4. Conclusions

In summary, we have demonstrated the investigation of highly sensitive and reliable pressure sensors based on a single-crystalline Si<sub>3</sub>N<sub>4</sub> nanobelt under various applied loading forces *via* C-AFM. The transverse piezoresistance coefficient  $\pi_{[1\bar{2}0]}$  of the nanobelts falls in the range of 2.2 to 8.8×10<sup>-11</sup> Pa<sup>-1</sup> with the applied forces from 25.6 to 135.3 nN. The relationship between the piezoresistance coefficients and applied forces is almost linear. The significant and linear decreases of the nanobelt resistances with the increase of the loading forces have been observed, which exhibit a variation of ~3

MΩ with a changed force of 1 nN, implying that the pressure sensors possess a high sensitivity. Stable and repeatable  $I$ - $V$  curves through multiple voltage sweeping have been achieved, suggesting that the Si<sub>3</sub>N<sub>4</sub> nanobelts pressure sensors are highly reliable. It is promising that current work might open a new door for the exploration of highly sensitive and reliable pressure sensors based on the single-crystalline Si<sub>3</sub>N<sub>4</sub> nanobelts.

### ***Acknowledgements***

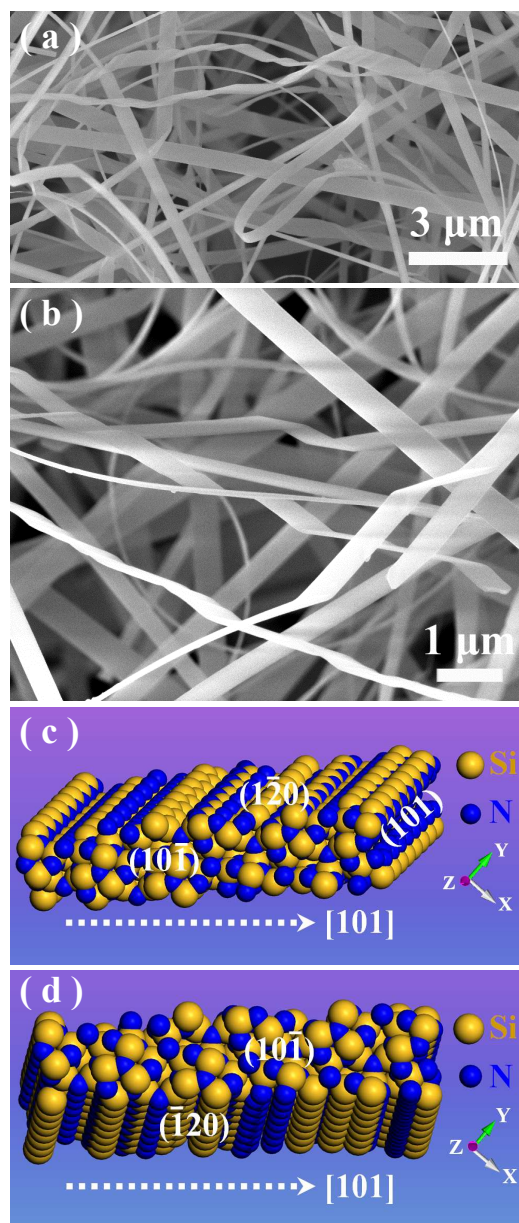
The work was financially supported by 973 program (Grant No. 2012CB326407), National Natural Science Foundation of China (NSFC, Grant Nos. 51372122 and 51202115), and Key Technology Program of Ningbo Municipal Government (Grant No. 2013B6007).

***Electronic Supplementary Information (ESI) available:*** The TEM characterizations of the Si<sub>3</sub>N<sub>4</sub> nanobelts. See DOI: 10.1039/b000000x/.

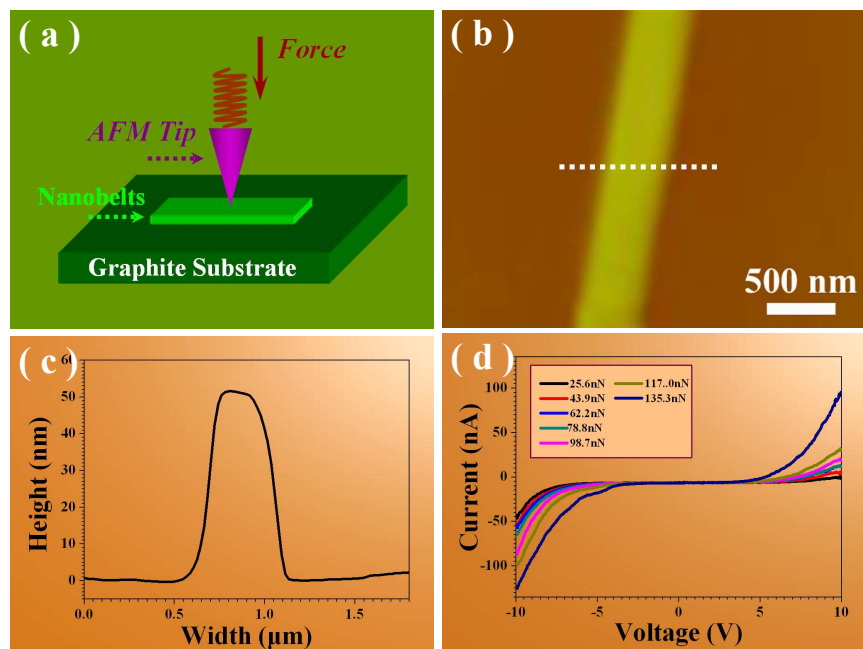
## References

1. R. He and P. Yang, *Nat. Nanotechnol.*, 2006, **1**, 42.
2. H. Tian, Y. Shu, Y.L. Cui, W.T. Mi, Y. Yang, D. Xie and T.L. Ren, *Nanoscale*, 2014, **6**, 699.
3. C. Stampfer, T. Helbling, D. Obergfell, B. Schöberle, M. Tripp, A. Jungen, S. Roth, V. Bright and C. Hierold, *Nano. Lett.*, 2006, **6**, 233.
4. C. Stampfer, A. Jungen, R. Linderman, D. Obergfell, S. Roth and C. Hierold, *Nano.Lett.*, 2006, **6**, 1449.
5. N. Hu, Y. Karube, C. Yan, Z. Masuda and H. Fukunaga, *Acta. Mater.*, 2008, **56**, 2929.
6. P. Neuzil, C. C. Wong and J. Reboud, *Nano. Lett.*, 2010, **10**, 1248.
7. X. Wang, J. Zhou, J. Song, J. Liu, N. Xu and Z. L. Wang, *Nano. Lett*, 2006, **6**, 2768.
8. Y. Yang, J. Qi, Y. Zhang, Q. Liao, L. Tang and Z. Qin, *Appl. Phys. Lett.*, 2008, **92**, 183117.
9. Y. Yang, J. Qi, W. Guo, Q. Liao and Y. Zhang, *CrystEngComm*, 2010, **12**, 2005.
10. Y. Yang, W. Guo, J. Qi and Y. Zhang, *Appl. Phys. Lett.*, 2010, **97**, 223107.
11. S. Lu, J. Qi, Z. Wang, P. Lin, S. Liu and Y. Zhang, *RSC Adv.*, 2013, **3**, 19375.
12. Y. Yang, J. Qi, W. Guo, Y. Gu, Y. Huang and Y. Zhang, *Phys. Chem. Chem. Phys.*, 2010, **12**, 12415.
13. F. Gao, J. Zheng, M. Wang, G. Wei and W. Yang, *Chem. Commun.*, 2011, **47**, 11993.
14. R. Shao, K. Zheng, Y. Zhang, Y. Li, Z. Zhang and X. Han, *Appl. Phys. Lett.*, 2012, **101**, 233109.
15. J. Bi, G. Wei, L. Wang, F. Gao, J. Zheng, B. Tang and W. Yang, *J. Mater. Chem. C*, 2013, **1**, 4514.
16. Y. Zhang, N. Wang, R. He, Q. Zhang, J. Zhu and Y. Yan, *J. Mater. Res.*, 2000, **15**, 1048.
17. G. Jing, H. Ji, W. Yang, J. Xu and D. Yu, *Appl. Phys. A*, 2006, **82**, 475.
18. F. Giorgis, *Appl. Phys. Lett.*, 2000, **77**, 522.
19. R. J. Sokel, *J. Phys. Chem. Solids*, 1980, **41**, 899.
20. R. Kärcher, L. Ley and R. Johnson, *Phys. Rev. B*, 1984, **30**, 1896.
21. R. Carson and S. Schnatterly, *Phys. Rev. B*, 1986, **33**, 2432.
22. F. Gao, W. Yang, Y. Fan and L. An, *Nanotechnology*, 2008, **19**, 105602.
23. W. Yang, Z. Xie, H. Miao, L. Zhang and L. An, *J. Phys. Chem. B*, 2006, **110**, 3969.
24. W. Yang, H. Wang, S. Liu, Z. Xie and L. An, *J. Phys. Chem. B*, 2007, **111**, 4156.
25. W. Yang, X. Cheng, H. Wang, Z. Xie, F. Xing and L. An, *Cryst. Growth Des.*, 2008, **8**, 3921.
26. W. Yang, F. Gao, G. Wei and L. An, *Cryst. Growth Des.*, 2009, **10**, 29.

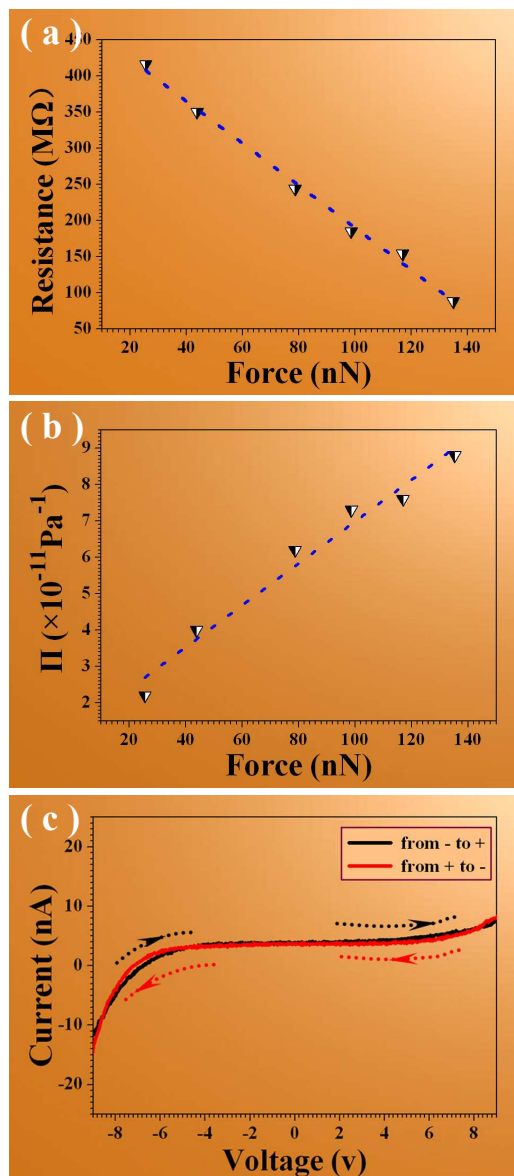
27. W. Yang, F. Gao, H. Wang, Z. Xie and L. An, *Cryst. Growth Des.*, 2008, **8**, 2606.
28. L. Zhang, H. Jin, W. Yang, Z. Xie, H. Miao and L. An, *Appl. Phys. Lett.*, 2005, **86**, 061908.
29. G. Maire, L. Vivien, G. Sattler, A. Kazmierczak, B. Sanchez, K. B. Gylfason, A. Griol, D. Marris-Morini, E. Cassan and D. Giannone, *Opt. Express*, 2008, **16**, 328.
30. Y. Chen, X. Zhang, Q. Zhao, L. He, Z. Xie and H. Wang, *Chem. Commun.*, 2012, **48**, 6016.
31. F. Gao, W. Yang, Y. Fan and L. An, *J. Solid State Chem.*, 2008, **181**, 211.
32. H. Ago, T. Kugler, F. Cacialli, W. R. Salaneck, M. S. P. Shaffer, A. H. Windle and R. H. Friend, *J. Phys. Chem. B*, 1999, **103**, 8116.
33. J. Wildoer, C. Harmans and H. Van Kempen, *Phys. Rev. B*, 1997, **55**, 16013.
34. K. L. Johnson, *Contact mechanics*, Cambridge University Press, 1985.
35. K. Liu, P. Gao, Z. Xu, X. Bai and E. Wang, *Appl. Phys. Lett.*, 2008, **92**, 213105.
36. J. Cao, X. Gong and R. Wu, *Phys. Rev. B*, 2007, **75**, 233302.
37. J. Milne, A. Rowe, S. Arscott and C. Renner, *Phys. Rev. Lett.*, 2010, **105**, 226802.
38. Z. Xiao, J. She, S. Deng and N. Xu, *J. Appl. Phys.*, 2011, **110**, 114323.
39. Y. Yang, Q. Liao, J. Qi, W. Guo and Y. Zhang, *Phys. Chem. Chem. Phys.*, 2010, **12**, 552.
40. S. M. Sze and K. K. Ng, *Physics of semiconductor devices*, John Wiley & Sons, Inc., 2006.



**Fig. 1** (a-b) Typical SEM images of the Si<sub>3</sub>N<sub>4</sub> nanobelts under different magnifications. (c-d) Crystal growth models for the nanobelts in different view angles.



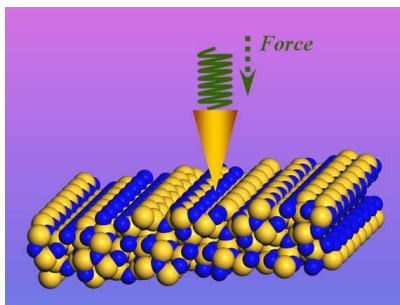
**Fig. 2** (a) A schematic diagram for the measurement of the piezoresistance in  $\text{Si}_3\text{N}_4$  nanobelt. (b) A representative AFM image of the nanobelt. (c) The corresponding height data recorded along the dashed white line marked in (b). (d) The typical  $I$ - $V$  curves recorded at different applied forces across the nanobelt.



**Fig. 3** (a) The relationship between the resistances of the  $\text{Si}_3\text{N}_4$  nanobelts and the applied forces. (b) The relationship between the piezoresistance coefficients of the nanobelts and the applied forces. (c) The  $I$ - $V$  characteristics of the nanobelt with bias voltage sweeping from negative to positive values and in turn under 43.9 nN.



## Table of Contents Entry



We report the piezoresistance behaviors in  $\text{Si}_3\text{N}_4$  nanobelts, which open a door for exploring highly sensitive and reliable pressure sensors.